JOURNAL OF MATERIALS SCIENCE **34** (1999) 6015–6025

Carbonization behavior of polyoxadiazole fibers and films

M. SHIOYA*, K. SHINOTANI‡
Department of Organic and Polymeric Materials, Tokyo Institute of Technology, 2-12-1 O-okayama, Meguro-ku, Tokyo 152-8552, Japan
E-mail: mshioya@o.cc.titech.ac.jp

A. TAKAKU
Life Culture Department, Seitoku University, 531 Sagamidai, Matsudo-shi, Chiba 271-8555, Japan

The carbonization behavior of polyoxadiazole (POD) fibers was investigated in comparison with that of films by using wide- and small-angle X-ray scattering, scanning electron microscopy and measurements of density, mass, volume and dimensional changes. On heat-treating POD fibers and films at a degradation temperature of about 500 °C, small-angle X-ray scattering from a long-period structure appeared and disappeared again, which indicated inhomogeneous progress of the scission of POD molecules. This accounted for the ability of this polymer to keep the macroscopic precursor geometry during carbonization in spite of yielding a graphitizing carbon. During the volume reduction process, the nuclei of the carbon layer stacks formed immediately after degradation of POD were piled up parallel to the material surface. This led to autonomous increase in the preferred orientation of the carbon layer stacks at higher temperatures. When the interlayer spacing decreased below 0.340 nm, the carbon layer stacks assumed three-dimensional regularity. The degree of the stacking regularity was higher for the films than the fibers. The macroscopic precursor geometry imposed a stronger restriction on the growth of the carbon layer stacks in the fibers than in the films.

1. Introduction

Carbons derived by heat-treating polyacrylonitrile (PAN) and cellulose fibers are non-graphitizing [1] and the development of graphite structure at a higher temperature is retarded. On the other hand, it is known that a polyoxadiazole (POD) film gives a graphitizing carbon which has the ability to acquire the graphite structure at a higher temperature. Murakami *et al*. [2, 3] have shown that carbon layer stacks with three-dimensional regularity are developed in a POD-based carbon film heat-treated at about 2000 °C and large and highly oriented nearly ideal graphite crystallites are produced above 2800 °C. As compared with various carbons derived from other heat-resistant condensation polymers, the POD-based carbon film shows a higher electric conductivity [4]. It is considered that POD is an attractive material also as the precursor of highly oriented carbon fibers.

Using POD for the precursor of carbon fiber is furthermore advantageous in shortening the carbon fiber production process because a preliminary oxidation process is not required due to the highly heat-resistant nature of POD [5]. For the production of PAN- and cellulose-based carbon fibers, a low-temperature thermal oxidation process is required in order to render the precursor fibers infusible prior to carbonization. The preliminary oxidation should be carried out under conditions requiring control of a considerable amount of heat evolution, and this makes the process extremely lengthy. On the other hand, POD can be converted to a carbon without the preliminary oxidation process, by keeping the macroscopic precursor geometry.

A number of studies have been performed on the spinning of POD mainly from the viewpoint of acquiring heat-resistant fibers. Frazer *et al*. [6–8] have obtained POD fibers by spinning polyhydrazide fibers and applying thermal conversion of polyhydrazide into POD. Imai [9] has obtained POD fibers by directly utilizing the synthesized POD solution as the wet-spinning solution. Jones and Soehngen [10] have successfully spun POD homopolymer fibers, which had been deemed to be difficult because of high viscosity, by using a dry-jet wet-spinning method. With respect to the production of POD-based carbon fibers, Dobrovol'skaya *et al*. [5] have investigated structural changes of POD fibers by heat-treatment up to 800 °C. It is

* Author to whom all correspondence should be addressed.
‡ *Present address*: Research and Development Division, Matsushita Electric Works, Ltd., 1048, Kadoma, Osaka 571, Japan.

considered, however, that the development of carbon structure is not sufficient at this temperature. Except for patent [11], relatively few reports have been published on the structure development of the POD-based carbon fiber at higher temperatures.

The present authors have been studying the structure of POD-based carbon fibers derived by the heat-treatment up to 2800 °C. The influences of the spinning method and its conditions on the structures of the as-spun fibers and the resulting carbon fibers have been reported in a previous paper [12]. The present authors have also investigated the difference in the microtextures between POD-based carbon fibers and the films [13]. This paper reports the results of more detailed investigations on the changes in the structure and the microtexture of POD fibers during heat-treatment in order to elucidate the carbonization behavior of POD fibers and the influences of the macroscopic precursor geometry. POD copolymer is used for the precursor material since it shows better processibility as compared with POD homopolymer. POD copolymer fibers are spun with a dry-jet wet-spinning method and heat-treated at high temperatures. These fibers are examined using wide- and small-angle X-ray scattering and scanning electron microscopy. For understanding the peculiar carbonization behavior of POD in which the macroscopic precursor geometry is kept during carbonization in spite of yielding a graphitizing carbon, measurements of density, mass, volume, fiber length and long-period structure are carried out around the degradation temperature of POD. These results are compared with those of POD-based carbon films and PAN- and pitch-based carbon fibers.

2. Experimental

2.1. Precursor materials

A random copolyoxadiazole with a chemical structure

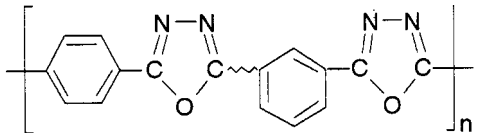

was synthesized from terephthalic acid, isophthalic acid and hydrazin sulfate in fuming sulfuric acid according to a method proposed by Imai [9]. A mixture of terephthalic acid and isophthalic acid by a weight ratio of 75/25 was added to a fuming sulfuric acid solution of hydrazin sulfate heated at 75 °C. The reaction mixture was stirred at 120 °C for 2 h and at 140 °C for an additional 2 h. The inherent viscosity of the synthesized POD measured at 30 °C and at a concentration of 2 kg m^{-3} was in the range from 0.12 to 0.18 m^3 kg^{-1}.

The POD was spun into fibers with a dry-jet wet-spinning method [12]. The fuming sulfuric acid solution of 7 wt % POD at 20 °C was extruded through a single-hole nozzle into a coagulation-bath consisting of an aqueous solution of 40 wt % sulfuric acid at 20 °C. The coagulated polymer was taken up on a winder at a linear velocity of four times that of extrusion. The wet, acid-containing fibers were soaked in a water bath at 95 °C and drawn to a desired draw ratio. The fibers were washed thoroughly and dried at 100 °C without allowing length shrinkage. The sample codes of these fibers, CD-1 and CD-3, indicate that the draw ratios were respectively 1 and 3, where the draw ratio was defined as the ratio of the fiber lengths after and before drawing.

The POD films were prepared by spreading a fuming sulfuric acid solution of 10 wt % POD on a glass plate heated at 70 °C and coagulating the extended films in an aqueous solution of 40 wt % sulfuric acid at room temperature. The coagulated films were removed from the glass plate and held with a rectangular frame in order to prevent length shrinkage during succeeding washing and drying processes. The films were washed in a water at 95 °C and dried in an ordinary atmosphere and in vacuum. The thickness of the films was in the range from 30 to 50 μm.

2.2. Heat-treatment

The POD fibers were heated to various temperatures up to 800 °C under a constant tensile stress of 2.62 MPa. The fibers heated up to 800 °C were further heated to various temperatures above 800 °C by sandwiching the fibers between two graphite plates and held at the maximum temperatures for 10 min. The heating rate of both treatments was 10 °C min^{-1} and after the treatments, the fibers were cooled spontaneously in the furnace. The heat-treatments below and above 1300 °C were made in a nitrogen and an argon atmosphere, respectively.

The heat-treatments of the films were carried out in one step, similarly to the heat-treatment of the fibers above 800 °C.

2.3. Measurements

2.3.1. Wide-angle X-ray diffraction of carbon layer stacks

The carbon layer stacks with graphite and turbostratic structures give quite different wide-angle X-ray diffraction (WAXD) patterns. Examples of the WAXD profiles of the carbon layer stacks with graphite and turbostratic structures which were observed for the pitch- and the PAN-based carbon fibers, respectively, are shown in Fig. 1. The (0 0 l) diffractions owing to the periodicity, perpendicular to the layer plane, of the stacking sequence are produced for both structures. For the graphite structure, the (h k l) diffractions separate into individual peaks with different values of l. For the turbostratic structure, however, the (h k l) diffractions appear as a tail of the (h k 0) diffraction owing to lack of the stacking regularity parallel to the layer plane. These diffractions are indexed as the (h k) diffraction. The broadening of the (h k) diffraction is in inverse proportion to the carbon layer extent, while its coefficient (Scherrer constant) varies depending on the degrees of the stacking regularity and the preferred orientation of the crystallites. For the three-dimensionally regular structure, the value of the Scherrer constant is 0.94. On the other hand, Warren has shown that this

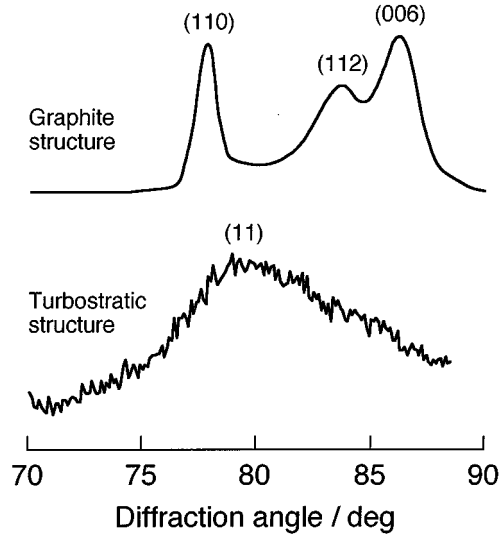

Figure 1 Equatorial WAXD profiles of pitch- and PAN-based carbon fibers comprising carbon layer stacks with graphite and turbostratic structures, respectively. WAXD profiles were normalized so that (1 1 0) and (1 1) diffraction peak intensities were equalized. Diffraction indices are shown in figure.

value for the randomly oriented carbon layer stacks with turbostratic structure is 1.84 [14]. Therefore, if the carbon layer extent is calculated using either of these two values without knowing the degrees of the stacking regularity and the preferred orientation of the crystallites, the maximum error can be as large as 96%. The present authors have shown that if the broadening of the ($h\,k$) diffraction at lower angle side of the peak is used instead of the full-width of the peak, the maximum error can be reduced to 10% for various degrees of the stacking regularity and the preferred orientation of the crystallites [15, 16]. The proposed equation to calculate carbon layer extent (L_a) is

$$L_a = \frac{0.26\lambda}{\sin\theta_p - \sin\theta_l} \quad (1)$$

where $2\theta_p$ is the peak diffraction angle, $2\theta_l$ the diffraction angle at half-maximum intensity on the lower angle side of the peak and λ the X-ray wavelength. The coefficient, 0.26, is the optimal value for the (1 1) diffraction. This equation will be used in this study.

The wide-angle X-ray diffraction from the carbon layer stacks was measured on aligned carbon fibers and stacked carbon films by using nickel-filtered Cu K_α radiation and a diffractometer. With the films, two types of specimens were prepared to permit the X-ray beam to impinge on the surface and the edges of the stacked films, and these specimens will be called through- and edge-view specimens, respectively. The diffractions from the edge-view specimen were scanned in the planes parallel and perpendicular to the film surface, and these geometries will be called the in-plane and normal edge-views, respectively. The diffraction angle scan of the (1 1) diffraction was made with the symmetrical transmission geometry, with respect to the diffraction peak, by using a position-sensitive proportional counter (PSPC). The diffraction angle scan of the (0 0 2) and the (0 0 4) diffractions and the azimuthal angle scan of the (0 0 2) diffraction were made with the symmetrical transmission geometry by using a proportional counter. On the intensity distributions measured as a function of the diffraction angle, the correction for the instrumental peak broadening was made by assuming that an observed peak was represented by the convolution of two Gaussian functions approximating a true diffraction and an instrumental peak broadening. The instrumental peak broadening was determined from the diffractions of Si single-crystal and SiO_2 powder standards.

From the meridional and the equatorial (1 1) diffractions of the fibers, the extent of carbon layers lying parallel to the fiber axis, measured in the fiber axis direction ($L_{a\parallel}$) and in the transverse direction ($L_{a\perp}$), were respectively calculated by using Equation 1. From the (1 1) diffraction of the through-view film specimens, the extent of carbon layers lying parallel to the film surface ($L_{a\parallel}$) was similarly calculated [17].

The average interlayer spacing ($d_{0\,0\,2}$) and the carbon layer stack height (L_c) were estimated from the (0 0 2) diffraction using the Bragg and Scherrer equations. From the (0 0 2) and (0 0 4) diffractions, when developed, the standard deviation (σ_c) and skewness parameter (τ_c) of the distribution of interlayer spacings were estimated [17]. The skewness parameter takes a positive value if the distribution of intelayer spacings has a longer tail at larger spacings, while it takes a negative value if the distribution has a longer tail at smaller spacings [18]. These parameters, determined for the fibers using the equatorial diffractions, concern the carbon layers lying parallel with the fiber axis. These parameters, determined for the films using the normal edge-view diffractions, concern the carbon layers lying parallel with the film surface.

From the relative intensities of the (1 1 0) and (1 1 2) diffractions, when developed, the stacking regularity parameter (R) was estimated [17]. This parameter is zero for the turbostratic structure, and increases with increasing stacking regularity up to unity for the regular ABAB type stacking sequence of the hexagonal graphite structure [18].

From the full-width at half-maximum intensity (FWHM) of the azimuthal angle scan of the (0 0 2) diffraction, the orientation parameter, which is defined as 1-FWHM/π, was estimated [17]. The orientation parameter determined for the fibers represents the distribution of the angles between carbon layer normals and the fiber axis. The orientation parameter, determined for the films using the edge-view specimens, represents the distribution of the angles between carbon layer normals and the normal of the film surface. The orientation parameter is zero if carbon layer normals are randomly distributed and increases up to unity for perfect orientation.

2.3.2. Small-angle X-ray scattering of microvoid

The small-angle X-ray scattering (SAXS) produced by the microvoids was measured using nickel-filtered Cu K_α radiation, a diffractometer and the PSPC without

attaching a height-limiting slit at the X-ray entrance window of the PSPC. The measurements were made on the same specimens used for WAXD using the 0-2θ transmission geometry as is ordinarily used for SAXS.

From the equatorial SAXS of the fibers, the magnification of the electron density difference at the periphery of microvoids (ε), the volume fraction of microvoids (v_p) and the parameters representing sizes of the microvoid cross-section perpendicular to the fiber axis such as the cross-section area (S_3), the inertial distance (D_3) and the chord length (l_2) were calculated. The parameter ε takes a value larger than unity if some material is included inside the microvoids or some element with a high electron density exists at the wall of the microvoids [19]. This parameter is unity if the microvoids are truly vacant holes.

From the normal edge-view SAXS of the films, the inertial distance (D_3) of the microvoids measured in the film thickness direction was calculated.

The precise definitions and estimation methods of these parameters have been described in other papers [17, 20, 21].

2.3.3. Small-angle X-ray scattering of long-period structure

The SAXS from the long-period structure was measured similarly to the measurements of SAXS from the microvoids. The meridional and the in-plane edge-view SAXS was measured for the fibers and the films, respectively.

2.3.4. Scanning electron microscopy

The gold-sputtered cross-sections of the fibers perpendicular to the fiber axis and those of the films perpendicular to the film surface were observed with scanning electron microscopy (SEM).

2.3.5. Density

The densities lower than 1600 kg m^{-3} were measured with a *n*-heptane/ethylene dibromide density gradient column, and those higher than 1600 kg m^{-3} by a sink-float method using a carbon tetrachloride/ethylene dibromide mixture. The measurements were made at 30 °C.

2.3.6. Dimensional changes

The volume of the specimens was calculated by dividing the mass with the density.

The length changes of the fibers during heat-treatment were measured on the fibers extended horizontally in an infrared tubular furnace. During the measurements, the fibers were heated at a rate of 10 °C min^{-1} up to 900 °C under constant tension in a nitrogen atmosphere. The fiber diameter was calculated from the volume and the length of the fibers by assuming a circular fiber cross-section.

The film thickness was measured with a micrometer.

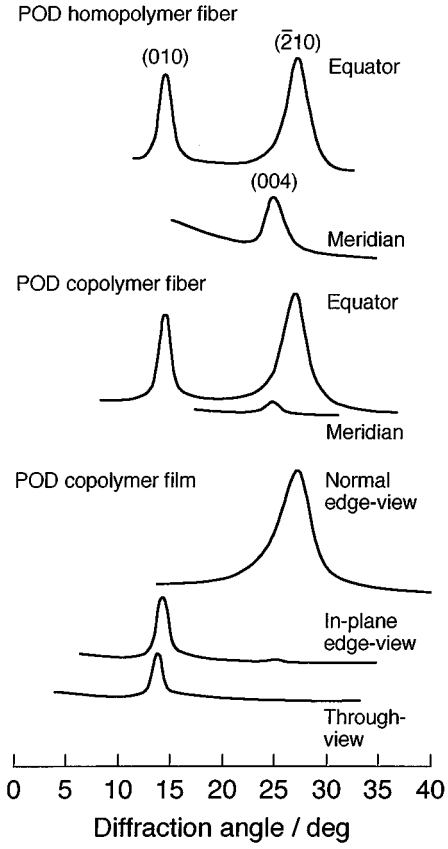

Figure 2 WAXD profiles of POD homopolymer fiber, POD copolymer fiber and POD copolymer film measured with symmetrical transmission geometry. In order to enhance crystallinity, fibers and film were preliminarily heated up to 450 °C. During this treatment, POD homopolymer fiber was kept at 380 °C for 1 h. WAXD profiles were normalized so that ($\bar{2}$ 1 0) diffraction peak intensities were equalized. Diffraction indices are shown in figure.

3. Results and discussion

3.1. Crystallite structure of precursor POD

The present authors have determined the lattice constants of the crystallites of the POD homopolymer synthesized from terephthalic acid and hydrazin sulfate. It has been obtained that the unit cell is monoclinic and $a = 0.939$ nm, $b = 0.639$ nm, $c = 1.468$ nm, $\alpha = \beta = 90°$ and $\gamma = 76.0°$ [22]. The end-to-end distance of two monomer units in the conformation allowing periodic displacements is estimated to be 1.5 nm, which corresponds to the *c*-axis length. From the density, the unit cell is estimated to contain three molecular chains.

The crystallite structure of the precursor POD copolymer used in this study was investigated with WAXD. The WAXD profiles of the POD copolymer fibers and films are compared with those of the POD homopolymer fibers in Fig. 2. It is seen that the POD copolymer fibers and films have similar crystallite structure as that of the POD homopolymer fibers. For the fibers, emergence of the (0 0 4) diffractions on the meridian indicates that the *c*-axis is preferentially oriented in the fiber axis direction. For the films, the absence of the (0 1 0) diffraction from the normal edge-view indicates that *b*-axis is nearly parallel to the film surface. The absence of the ($\bar{2}$ 1 0) diffraction from the in-plane edge- and through-views indicates that the normal of the ($\bar{2}$ 1 0) plane is nearly in the film thickness

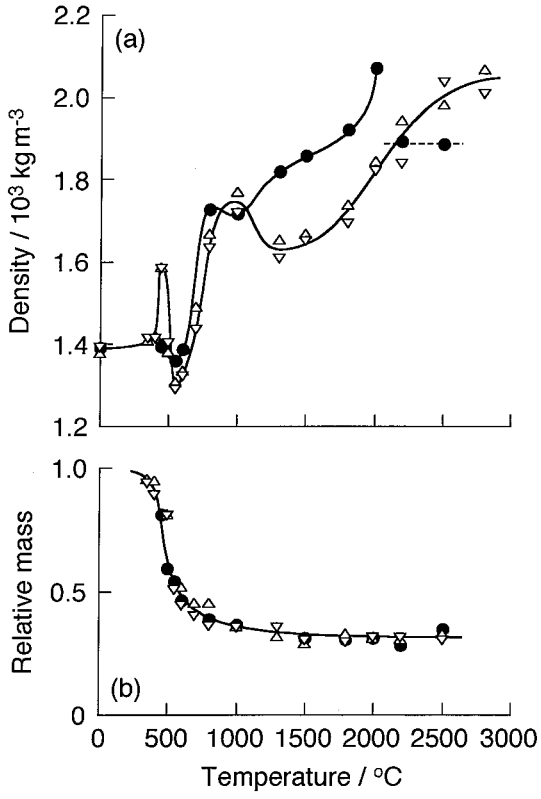

Figure 3 (a) Density and (b) relative mass versus heat-treatment temperature. Precursor materials are (△) CD-1 fiber, (▽) CD-3 fiber and (●) POD film.

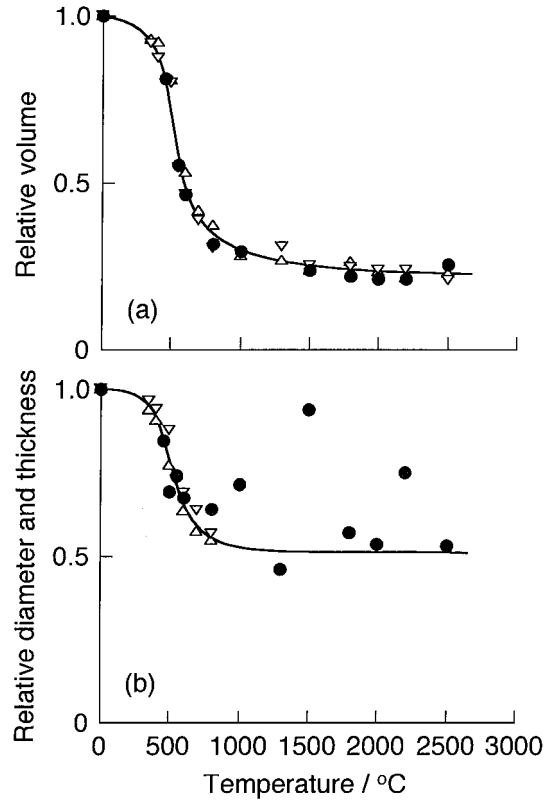

Figure 4 (a) Relative volume, (b) relative fiber diameter and relative film thickness versus heat-treatment temperature. Precursor materials are (△) CD-1 fiber, (▽) CD-3 fiber and (●) POD film.

direction. Since the *b*-axis and the normal of the $(\bar{2}\,1\,0)$ plane make an angle of 58.8°, there may be an inclination of the *b*-axis from the direction parallel to the film surface and/or the normal of the $(\bar{2}\,1\,0)$ plane from the film thickness direction. The *c*-axis is considered to be parallel to the film surface.

3.2. Pyrolytic degradation of POD

The changes in density, mass, volume and dimensions of the POD fibers and films with increasing heat-treatment temperature are shown in Figs 3 and 4. A large scatter of film thickness is due to an uneven surface texture. The POD fibers and films show a rapid reduction of mass and dimensions in a narrow temperature region at about 500 °C.

Murakami *et al.* [23] have proposed the following chemical changes which take place at the degradation temperature of POD: The oxadiazole rings in POD are decomposed, and *p*-dicyanobenzene and *p*-aminocyanobenzene are released causing mass reduction. In the residues, benzen compounds having a −N=C=O group are formed and these compounds are coupled into carbodiimides (−N=C=N−). The carbodiimides react with each other by the cyclization reactions forming heterocyclic rings. At high temperatures, the heterocyclic rings change to nitrogen-containing aromatic polycyclic compounds.

The structural changes taking place around the degradation temperature is sensitively reflected in the fiber length change as shown in Fig. 5. It is found that there are two characteristic temperature regions, one from about 350 to 500 °C and the other higher than 500 °C.

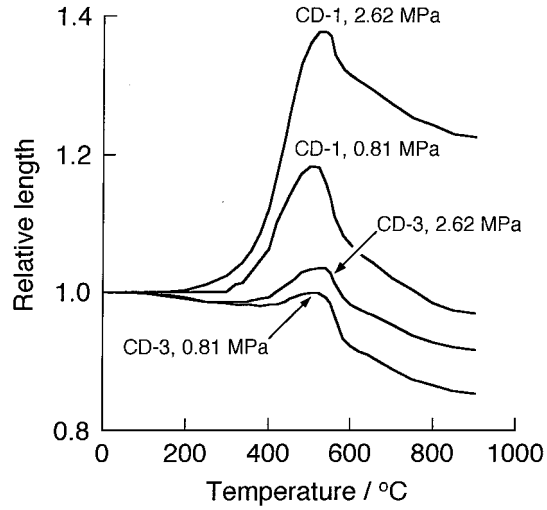

Figure 5 Changes in relative fiber length with heat-treatment temperature under tensile stresses. Precursor fibers and applied stresses are shown in figure.

In the temperature region from 350 to 500 °C, the fibers become extensible even under a small tensile stress, and the relative fiber length shows a maximum at about 500 °C. The fibers prepared with lower draw ratios show larger values of the maximum relative fiber length. As shown in Fig. 3, significant and transitory increase in fiber density is brought about by heat-treatment at 450 °C. Simultaneously, the WAXD from the POD crystallites was observed to increase. These results indicate that in the temperature region from 350 to 500 °C, the degradation reaction of the oxadiazole ring promotes the rearrangement of POD molecules.

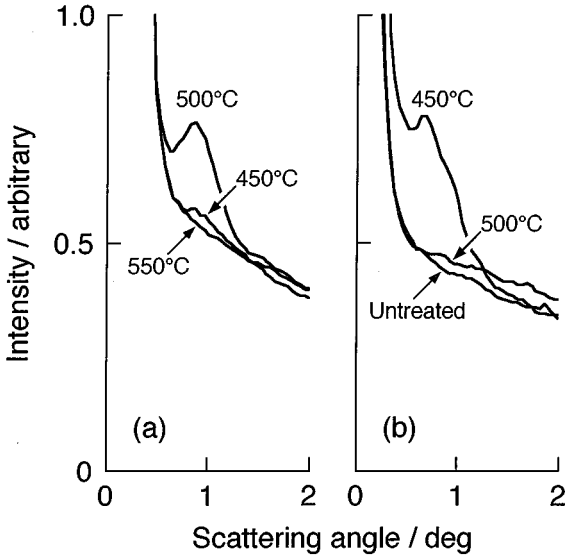

Figure 6 (a) Meridional SAXS profiles of CD-3 fiber and (b) in-plane edge-view SAXS profiles of POD film. Heat-treatment temperatures are shown in figure.

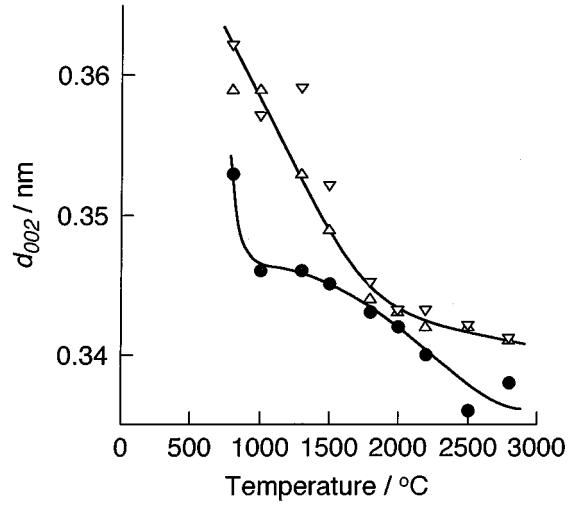

Figure 7 Average interlayer spacing (d_{002}) versus heat-treatment temperature. Precursor materials are (△) CD-1 fiber, (▽) CD-3 fiber and (●) POD film.

At about 500 °C, the fibers under tensile stress turn to shrink. At this temperature, the mass reduction nearly finishes, and the density begins to increase. The length shrinkage arises as a result of the volume contraction of the fibers due to the formation of the nitrogen-containing aromatic polycyclic compounds and their stacks.

Since the ability of POD to keep the macroscopic precursor geometry during carbonization is considered to be closely related to the structural changes taking place around the degradation temperature, more investigations were carried out using SAXS. Fig. 6 shows the SAXS profiles of the POD-based fibers and films heat-treated at temperatures from 450 to 550 °C. It is found that a long-period structure transitorily appears in this temperature region. The long-periods are about 10 and 13 nm for the fibers and the films, and are aligned in parallel to the fiber axis and the film surface, respectively.

The cause of the transitory development of the SAXS peak is considered to be as follows: Periodical arrangements of the crystalline and amorphous regions have been formed during the coagulation process of POD, though the electron density difference between these two regions is too small to produce a SAXS peak. The degradation reactions proceed at different rates between these two regions, and the density decreases at a faster rate in one or other of the two regions. The electron density difference thereby becomes contrasted enough to produce the SAXS peak. Due to continued formation of heterocyclic rings in both regions, the density difference between these regions is reduced again, resulting in disappearance of the SAXS peak.

The carbonization of the organic materials proceeds via either gas, liquid or solid phases depending on the melting, boiling and degradation temperatures of the material. Under ordinary pressures, graphitizing carbons are usually yielded through gas or liquid phase carbonization since the rearrangement of the structure necessary to acquire the near-parallel orientation of the nuclei of the carbon layer stacks is allowed in gas or liquid state. It is considered that the inhomogeneous progress of the scission of POD molecules accounts for the ability of this polymer to keep the macroscopic precursor geometry during carbonization in spite of yielding a graphitizing carbon.

3.3. Development of carbon structure

WAXD characteristic of carbon layer stacks became evident at about 800 °C. The average interlayer spacing (d_{002}) of the carbon layer stacks in the POD-based carbon films decreases with increasing heat-treatment temperature and takes a value close to that of graphite, 0.335 nm, at above 2500 °C as shown in Fig. 7. With the POD-based carbon fibers, however, the reduction of the interlayer spacing is retarded at 2000 °C.

If the average interlayer spacing, instead of the heat-treatment temperature, is adopted as a measure of the degree of carbonization, unique relationships, independent of the types and the macroscopic geometry of the precursor materials, can be obtained between some of the crystallite parameters and the degree of carbonization. The standard deviation (σ_c) and the skewness parameter (τ_c) of the distribution of interlayer spacings, the stacking regularity parameter (R), the carbon layer stack height (L_c), the carbon layer extents ($L_{a\parallel}$ and $L_{a\perp}$) and the orientation parameter for the POD-based carbon fibers and films are plotted against average interlayer spacing in Figs 8–10. In these figures, the crystallite parameters for the PAN- and pitch-based carbon fibers cited from Ref. [17] are shown together. The layer extent of the films heat-treated above 2500 °C could not be accurately determined since the (1 1) diffraction peak was sharper than the diffraction from the standard crystals.

In Figs 8–10, the following aspects are commonly observed independent of the precursor materials: Reduction of the average interlayer spacing below 0.345 nm begins when the crystallite sizes begin to grow markedly. Simultaneously, the distribution of the

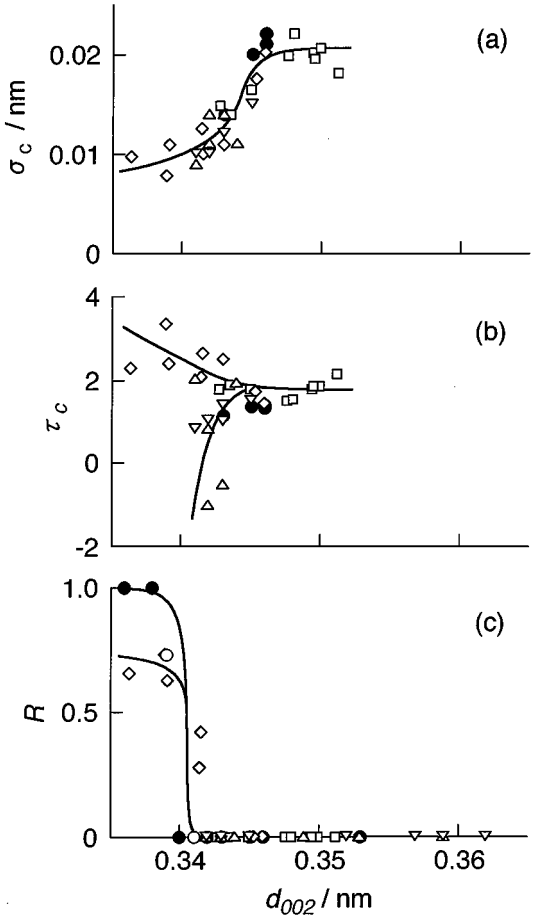

Figure 8 (a) Standard deviation (σ_c) and (b) skewness parameter (τ_c) of interlayer spacing distribution and (c) stacking regularity parameter (R) versus average interlayer spacing (d_{002}). Precursor materials are (△) CD-1 fiber, (▽) CD-3 fiber, (○) POD fiber taken up at linear velocity of twice that of extrusion and drawn to draw ratio of four [12], (●) POD film, (□) PAN fiber and (◇) pitch fiber.

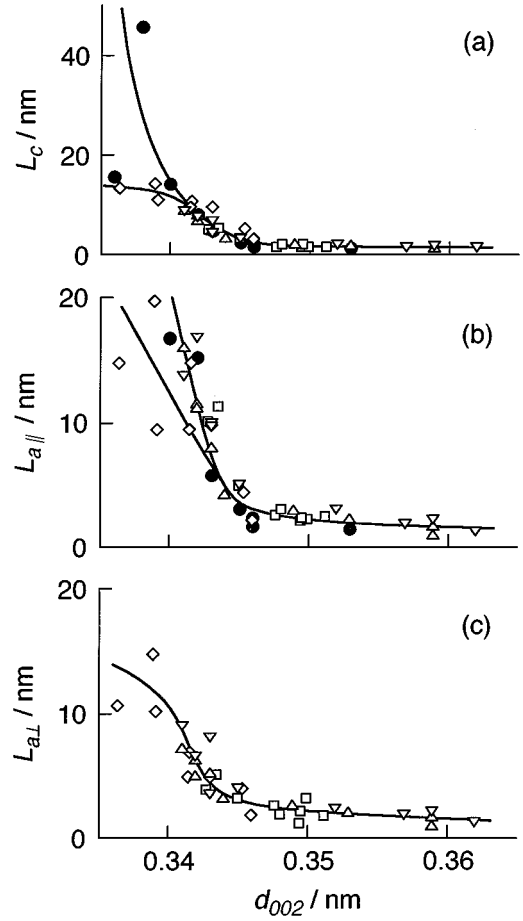

Figure 9 (a) Carbon layer stack height (L_c), (b) carbon layer extent parallel to fiber axis and film surface ($L_{a\parallel}$) and (c) carbon layer extent perpendicular to fiber axis ($L_{a\perp}$) versus average interlayer spacing (d_{002}). Precursor materials are (△) CD-1 fiber, (▽) CD-3 fiber, (●) POD film, (□) PAN fiber and (◇) pitch fiber.

interlayer spacings notably decreases. Significant increase in the stacking regularity for the POD- and pitch-based carbons takes place when the average interlayer spacing decreases to 0.340 nm. The region of the average interlayer spacing where the stacking regularity develops for the POD-based carbons almost coincides with that region reported for the cokes from petroleum [24] and polyvinylchloride [25], below about 0.342 nm.

The orientation parameters for the POD-based carbon fibers and films increase autonomously without stretching the materials during heat-treatment, and the increase is pronounced in the region where the crystallite sizes grow markedly. Although the orientation parameter for the fibers and the films show a unique dependence on the average interlayer spacing, it should be noted that the carbon layer normals distribute in different manners around the symmetry axes. That is, the carbon layer normals in the fibers are preferentially oriented perpendicularly to the fiber axis while those of the films are parallel to the normal of the film surface.

The aspects which depend on the types or the macroscopic geometry of the precursor materials are as follows: the changes in the crystallite parameters as a function of the heat-treatment temperature; the skewness of the interlayer spacing distribution; the values of the stacking regularity parameter reached at a high temperature; and the anisotropy of the crystallite sizes. That is, the layer stacking of the POD-based carbon films is more ordered than the POD- and pitch-based carbon fibers, and approaches that of graphite. For the fibers, the layer extent is larger in the fiber axis direction than in the transverse direction.

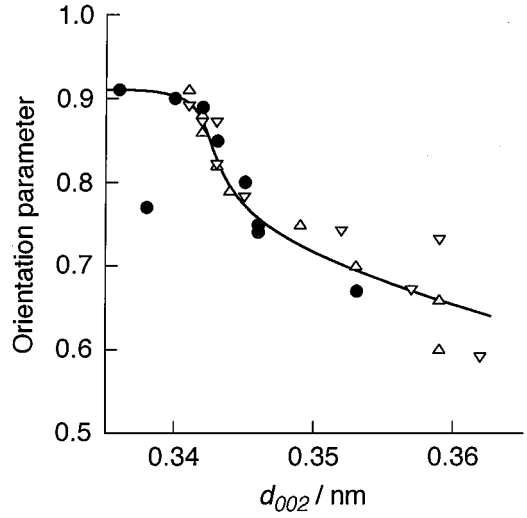

Figure 10 Orientation parameter versus average interlayer spacing (d_{002}). Precursor materials are (△) CD-1 fiber, (▽) CD-3 fiber and (●) POD film.

Carbon fibers and films were also prepared from POD homopolymer [12] by heat-treating at 1300 and 2800 °C, and their crystallite parameters were compared with those of the carbons from POD copolymer. No marked difference in the crystallite structure attributable to the difference in the composition of POD was detected.

Besides cellulose, PAN and pitch fibers and POD films [2, 3], various polymeric materials such as aromatic polyamide fibers [26, 27], poly(*p*-phenylene benzobisthiazole) fibers [28] and polyimide films with different chemical structures [29–33] have been tested for the applicability as the precursors of carbon fibers and films. The similarity in the carbonization behavior of these polymers with POD is that the loss of mass takes place in a relatively narrow temperature range around 500–600 °C for aromatic polyamide [27] and polyimides [29] and around 700–800 °C for poly(*p*-phenylene benzobisthiazole) [28]. It is considered that after decomposition of the starting molecules, POD, polyamides and polyimides follow a similar carbonization path since carbodiimides are formed as intermediates during decomposition of these starting molecules and the heterocyclic rings are formed therefrom [23, 29]. The differences in the chemical structure of the starting molecules, molecular orientation [34–36] and the processing conditions [37], however, cause variation in the structure and properties of the resulting carbons. As a result, the POD-based carbon contains a larger amount of nitrogen than the polyimide-based carbon when compared at the heat-treatment temperature of 1400 °C [29, 38]. The interlayer spacing of the carbon heat-treated at 2500 °C is the smallest for the POD-based carbon as compared with the carbons derived from polyamideimide, aromatic polyamide, polyimide and polybenzimidazole [39]. The electrical conductivity of carbons heat-treated at 1000 and 2500 °C is also the highest for the POD-based carbon among these carbons [39].

3.4. Development of microvoids

The microvoids in POD-based carbon fibers gave a streak-like SAXS pattern extending along the equator. This suggests that these microvoids are of needle-like shape, oriented in the fiber axis direction. The microvoids in POD-based carbon films gave a streak-like edge-view SAXS pattern extending perpendicularly to the film surface, while the through-view SAXS is limited in a very low scattering angle region. This suggests that these microvoids are of plate-like shape, orienting their flat surfaces parallel to the film surface.

The magnification of the electron density difference at the periphery of microvoids (ε) decreases with decreasing average interlayer spacing as shown in Fig. 11a for the carbon fibers from POD, PAN [17] and pitch [17]. Thus, it is known that the microvoids become truly vacant holes with increasing temperature.

It was obtained that the microvoid volume fraction in POD-based carbon fibers takes two maxima at the heat-treatment temperatures of 1300 and 2000 °C. The increase in the microvoid volume fraction at 1300 °C

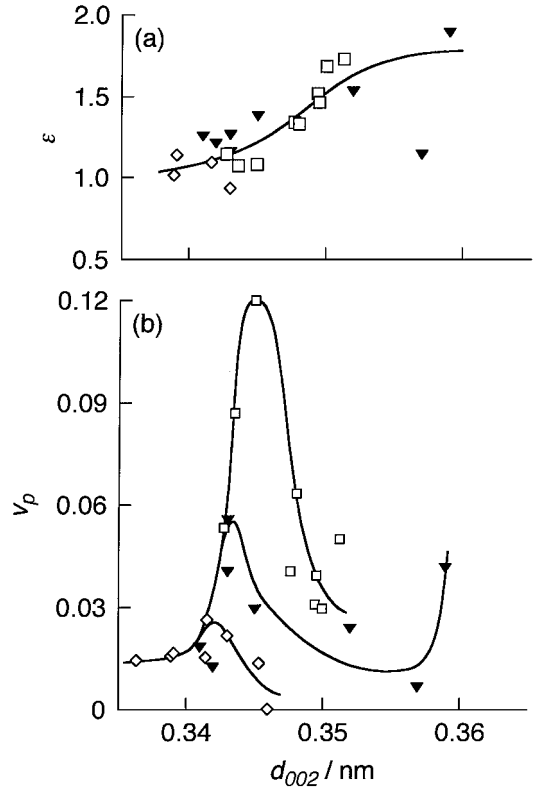

Figure 11 (a) Magnification of electron density difference at periphery of microvoids (ε) and (b) microvoid volume fraction (v_p) versus average interlayer spacing (d_{002}). Precursor materials are (▼) CD-3 fiber, (□) PAN fiber and (◇) pitch fiber.

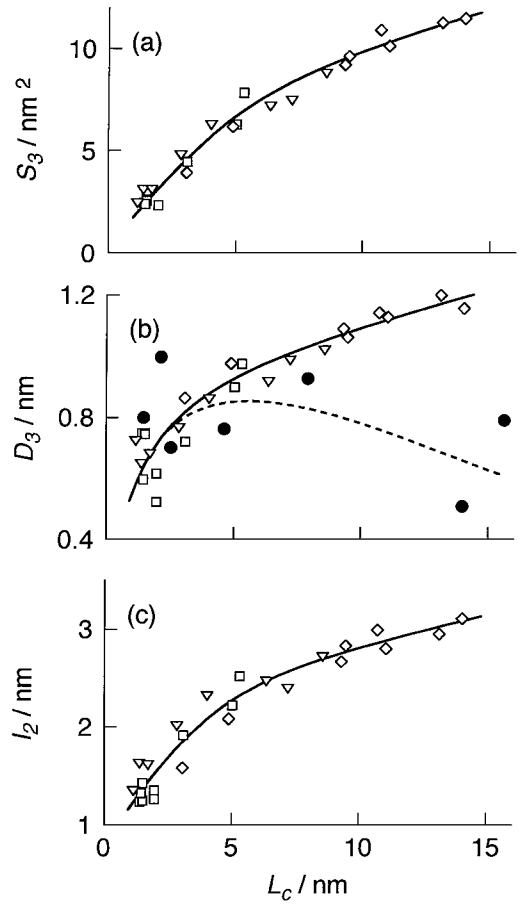

Figure 12 (a) Cross-section area (S_3), (b) inertial distance (D_3) and (c) chord length (l_2) versus carbon layer stack height (L_c). Precursor materials are (▽) CD-3 fiber, (●) POD film, (□) PAN fiber and (◇) pitch fiber. Microvoid sizes were measured perpendicularly to fiber axis for fibers and in film thickness direction for films.

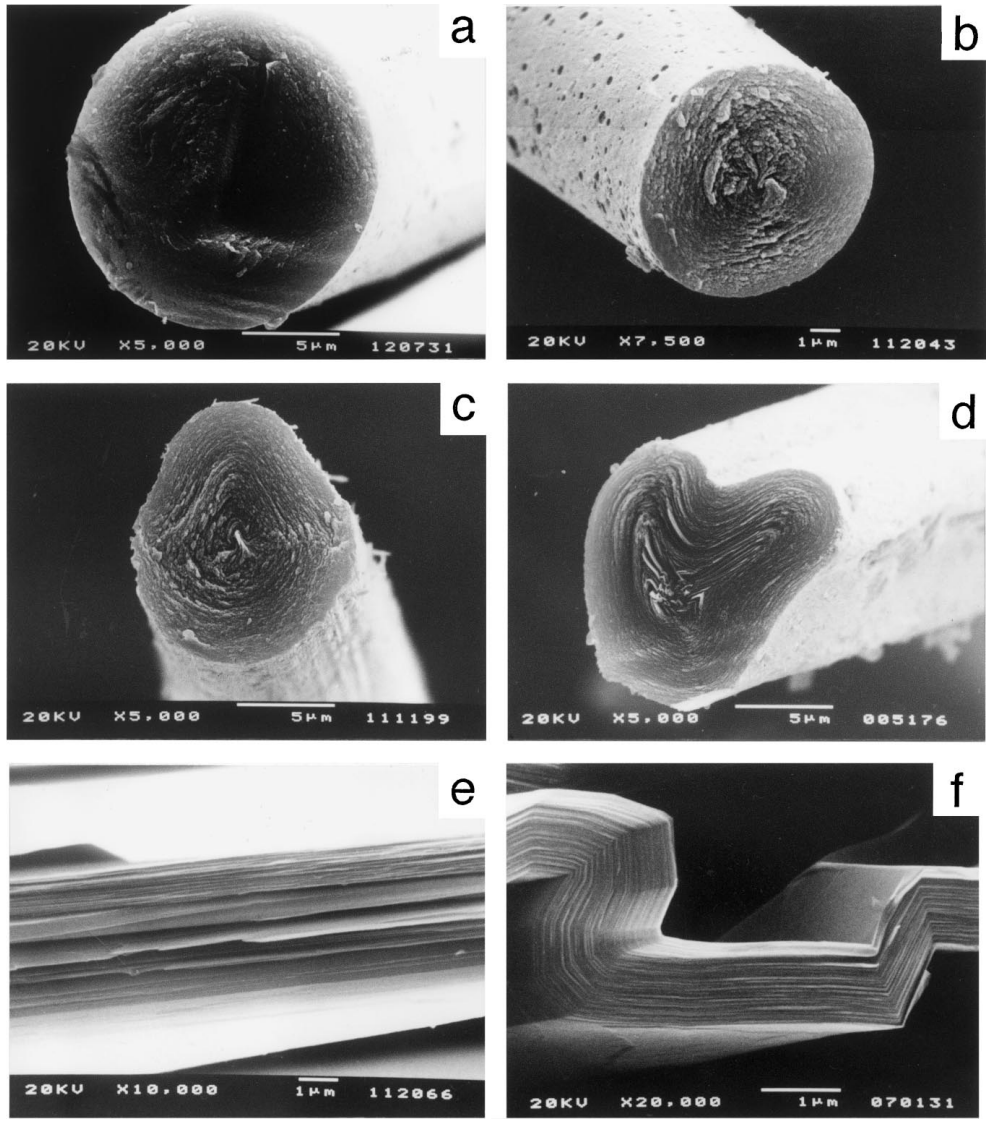

Figure 13 SEM photographs of cross-sections, perpendicular to fiber axis, of CD-3 fibers heat-treated at (a) 1300, (b) 1800, (c) 2200 and (d) 2800 °C, and those, perpendicular to film surface, of POD films heat-treated at (e) 2200 and (f) 2800 °C.

accounts for the decrease in the fiber density at this temperature as shown in Fig. 3. On the other hand, the fiber density does not decrease at 2000 °C because of a marked growth of the crystallites at this temperature. By plotting the microvoid volume fraction (v_p) for the carbon fibers from POD, PAN [17] and pitch [17] against the average interlayer spacing as in Fig. 11b, it is known that the microvoid volume fraction increases with decreasing average interlayer spacing from about 0.350 to 0.345 nm. After the microvoid fraction takes a maximum, it decreases concomitantly with a marked growth of the crystallite sizes. It is considered that the rearrangement of the structure is allowed in this region, promoting the significant growth of crystallites and the decrease in the microvoid volume fraction.

For carbon fibers from POD, PAN [17] and pitch [17], the cross-section area (S_3), the inertial distance (D_3) and the chord length (l_2) of the microvoid cross-section perpendicular to the fiber axis are uniquely correlated to the carbon layer stack height as shown in Fig. 12. The microvoid sizes increase at a faster rate with increasing layer stack height up to about 6 nm, and at a slower rate beyond this layer stack height. Since the microvoid volume fraction decreases when the layer stack height increases beyond 6 nm, the increase in the microvoid sizes in this region is considered to be due to the disappearance of the microvoids with smaller sizes. In contrast to the fibers, the thickness of the microvoids in the films, measured in the film thickness direction, tends to decrease with the growth of the crystallites as shown in Fig. 12b.

3.5. Development of lamellar texture

The SEM photographs of the cross-sections of the POD-based carbon fibers and films, perpendicular to the fiber axis and the film surface respectively, are shown in Fig. 13.

The fibers heat-treated at 1300 °C show apparently a smooth cross-section as shown in Fig. 13a, while small granular domains were observed at a high magnification. The granular texture becomes evident with increasing temperature. At 1800 °C, the granular texture changes into a circumferentially oriented lamellar texture as shown in Fig. 13b. The lamellae grow more distinctly with increasing temperature. Polarizing optical

microscopy showed that the carbon layers are aligned in parallel with the lamellae revealed in the SEM photographs. At 2200 °C, the circular cross-section of the fibers changes into a triangular shape as shown in Fig. 13c. The straight portions of the contour extends with increasing temperature as shown in Fig. 13d.

With the films, the granular texture appears at 1000 °C, and the lamellar texture appears at 1300 °C. The lamellae oriented in parallel with the film surface grow more distinctly with increasing temperature as shown in Fig. 13e. At 2800 °C, sharp kinks of the lamellae are produced as shown in Fig. 13f.

From the results shown so far, the changes in the structure and the microtexture of the POD-based carbons can be summarized as follows: At the temperature of about 500 °C, the gaseous compounds formed by the degradation of POD are released from the material and the volume reduction takes place. Simultaneously, the nuclei of the carbon layer stacks formed in the residues are piled up in parallel to the material surface. This leads to the preferred orientation of the carbon layer stacks yielded at higher temperatures. With the growth of the crystallites at higher temperatures, the wrinkled and wavy carbon layers are flattened, resulting in the reduction of the interlayer spacing. The lamellar texture starts appearing when the crystallite sizes begin to increase markedly. This takes place at the average interlayer spacing of about 0.345 nm for both fibers and films. Since the curved layer stacks formed in the fibers at earlier stages of heat-treatment tend to change into the planar layer stacks by releasing the strain energy, the circular cross-section of the fibers changes into a triangular one. Reduction of the interlayer spacing with increasing temperature is retarded when deformation of the fiber cross-section begins to take place. This suggests that the macroscopic precursor geometry imposes restriction on the development of carbon structure. The restriction from the macroscopic precursor geometry is also revealed in the anisotropic growth of the layer extents in the fibers. With the films, the planar layer stacks can easily grow parallel to the film surface, and the crystallites grow larger in the films than in the fibers at a given temperature. The three-dimensional regularity of the carbon layer stacks develops in the fibers and the films when the average interlayer spacing decreases below 0.340 nm. The formation of the kinks of the lamellae in the films may result from strains locally accumulated owing to the increases in the crystallite sizes and stacking regularity. The formation of the kinks and the vacant spaces between the kinked lamellae causes extraordinary decreases in the orientation parameter and the bulk density.

4. Conclusions

The peculiarity of POD to keep the macroscopic precursor geometry during carbonization in spite of yielding a graphitizing carbon was attributed to inhomogeneous progress of the scission of POD molecules between the amorphous and the crystalline regions. The nuclei of the carbon layer stacks formed immediately after degradation of POD were piled up in parallel to the material surface during volume reduction process of the materials. This led to the autonomous increase in the preferred orientation of the carbon layer stacks at higher temperatures.

The reduction of the average interlayer spacing below 0.345 nm for the POD-based carbons begun when the sizes of the carbon layer stacks begun to grow markedly, and the three-dimensional regularity of the carbon layer stacks was developed when the average interlayer spacing decreased below 0.340 nm. The carbon layer stacking in the POD-based carbon films was more ordered than in the POD- and pitch-based carbon fibers. The macroscopic precursor geometry imposed a stronger restriction on the crystallite growth for the POD-based carbon fibers as compared with the films. This was revealed also in the distortion of the fiber cross-section from a circular shape into a triangular shape and in the retardation of the reduction of the interlayer spacing for the fibers.

The microvoids in POD-based carbon fibers were of needle-like shape, oriented in the fiber axis direction. The microvoids in the films were of plate-like shape, orienting their flat surfaces in parallel to the film surface. The sizes of the microvoids in POD-based carbon fibers increased with increasing crystallite sizes, whereas the microvoid volume fraction decreased in a high temperature region where rearrangement of the structure allowing marked growth of the crystallite sizes took place.

Acknowledgements

The authors wish to thank Professor E. Yasuda, Tokyo Institute of Technology and Mr. Y. Takahashi, Nisshinbo Industries Inc. for specimen preparation. Thanks are also due to Mr. T. Chiba, Tokyo Institute of Technology for the SEM observation.

References

1. R. E. FRANKLIN, *Proc. R. Soc. London* **A209** (1951) 196.
2. M. MURAKAMI, K. WATANABE and S. YOSHIMURA, *Appl. Phys. Lett.* **48** (1986) 1594.
3. M. MURAKAMI and S. YOSHIMURA, *Synth. Met.* **18** (1987) 509.
4. M. MURAKAMI, H. YASUJIMA and S. YOSHIMURA, *Polym. Prepr. Jpn.* **34** (1985) 2949.
5. I. P. DOBROVOL'SKAYA, Z. YU. CHEREISKII and I. M. STARK, *Polym. Sci. U.S.S.R.* **23** (1981) 1398.
6. A. H. FRAZER and F. T. WALLENBERGER, *J. Polym. Sci. Part A* **2** (1964) 1171.
7. A. H. FRAZER and T. A. REED, *ibid. Part C* **19** (1967) 89.
8. A. H. FRAZER and D. R. WILSON, *Appl. Polym. Symp.* **9** (1969) 89.
9. Y. IMAI, *J. Appl. Polym. Sci.* **14** (1970) 225.
10. R. S. JONES and J. W. SOEHNGEN, *ibid.* **25** (1980) 315.
11. H. M. EZEKIL and R. G. SPAIN, US Patent no 3.528.774 (1970).
12. K. SHINOTANI, H. ISHII, M. SHIOYA, T. KIKUTANI and A. TAKAKU, *Sen'i Gakkaishi* **47** (1990) 234.
13. K. SHINOTANI, M. SHIOYA, T. KIKUTANI and A. TAKAKU, *ibid.* **48** (1992) 379.
14. B. E. WARREN, *Phys. Rev.* **59** (1941) 693.
15. M. SHIOYA and A. TAKAKU, *J. Appl. Cryst.* **22** (1989) 222.
16. *Idem., Tanso* **139** (1989) 189.
17. A. TAKAKU and M. SHIOYA, *J. Mater. Sci.* **25** (1990) 4873.
18. M. SHIOYA and A. TAKAKU, *Carbon* **28** (1990) 165.

19. A. TAKAKU and M. SHIOYA, *J. Mater. Sci.* **21** (1986) 4443.
20. M. SHIOYA and A. TAKAKU, *J. Appl. Phys.* **58** (1985) 4074.
21. M. SHIOYA, M. NAKATANI, H. KITANO, A. TAKAKU, Y. ARAKI, Y. TAKAHASHI and T. SUZUKI, *Carbon* **34** (1996) 1229.
22. M. SHIOYA, K. SHINOTANI, T. KIKUTANI and A. TAKAKU, in Proceedings of 18th Annual Meeting of the Carbon Society of Japan, Saitama, Japan, 1991, p. 1B05.
23. M. MURAKAMI, Y. YUMOTO, S. MIZOGAMI, H. YASUJIMA, S. NAITOH and S. YOSHIMURA, *J. Polym. Sci. Part A* **28** (1990) 1483.
24. M. INAGAKI, *Tanso* **53** (1968) 61.
25. M. INAGAKI, Y. MURASE and T. NODA, *ibid.* **54** (1968) 80.
26. H. M. EZEKIEL, *Appl. Polym. Symp.* **9** (1969) 315.
27. I. TOMIZUKA, Y. ISODA and Y. AMAMIYA, *Tanso* **106** (1981) 93.
28. H. JIANG, P. DESAI, S. KUMAR and A. S. ABHIRAMAN, *Carbon* **29** (1991) 635.
29. A. BURGER, E. FITZER, M. HEYM and B. TERWIESCH, *ibid.* **13** (1975) 149.
30. M. INAGAKI, S. HARADA, T. SATO, T. NAKAJIMA, Y. HORINO and K. MORITA, *ibid.* **27** (1989) 253.
31. M. INAGAKI, L. MENG, T. IBUKI, M. SAKAI and Y. HISHIYAMA, *ibid.* **29** (1991) 1239.
32. M. INAGAKI and K. SAKAMOTO, *J. Mat. Res.* **6** (1991) 1108.
33. Y. HISHIYAMA, Y. KABURAGI, A. YOSHIDA and M. INAGAKI, *Carbon* **31** (1993) 773.
34. M. INAGAKI, M. SATO, T. TAKEICHI, A. YOSHIDA and Y. HISHIYAMA, *ibid.* **30** (1992) 903.
35. H. HATORI, Y. YAMADA and M. SHIRAISHI, *ibid.* **30** (1992) 763.
36. T. TAKEICHI, Y. KABURAGI, Y. HISHIYAMA and M. INAGAKI, *ibid.* **33** (1995) 1621.
37. M. INAGAKI, Y. HISHIYAMA and Y. KABURAGI, *ibid.* **32** (1994) 637.
38. M. MURAKAMI, H. YASUJIMA, Y. YUMOTO, S. MIZOGAMI and S. YOSHIMURA, *Solid State Comm.* **45** (1983) 1085.
39. S. YOSHIMURA, M. MURAKAMI and H. YASUJIMA, in "Polymers for High Technology: Electrics and Photonics," edited by M. J. Bowden and S. R. Turner (American Chemical Society, Washington, DC, 1987) chap. 49, p. 584.

Received 8 December 1998
and accepted 11 June 1999